Letter

Transparent Josephson junctions in higher-order topological insulator WTe_2 via Pd diffusion

Martin Endres [1,*] Artem Kononov [1] Michael Stiefel,[2] Marcus Wyss [3] Hasitha Suriya Arachchige,[4] Jiaqiang Yan [4,5] David Mandrus,[4,5,6] Kenji Watanabe [7] Takashi Taniguchi,[7] and Christian Schönenberger [1,3,†]

[1]*Department of Physics, University of Basel, Klingelbergstrasse 82, 4056 Basel, Switzerland*
[2]*Laboratory for Nanoscale Material Science, Swiss Federal Laboratories for Material Science and Technology, EMPA, Überlandstrasse 129, 8600 Dübendorf, Switzerland*
[3]*Swiss Nanoscience Institute, University of Basel, Klingelbergstrasse 82, 4056 Basel, Switzerland*
[4]*Department of Physics and Astronomy, University of Tennessee, Knoxville, Tennessee 37996, USA*
[5]*Material Science and Technology Division, Oak Ridge Laboratory, Oak Ridge, Tennessee 37831, USA*
[6]*Department of Materials Science and Engineering, University of Tennessee, Knoxville, Tennessee 37996, USA*
[7]*National Institute for Materials Science, 1-1 Namiki, Tsukuba 305-0044, Japan*

(Received 30 May 2022; revised 25 July 2022; accepted 8 August 2022; published 29 August 2022)

Highly transparent superconducting contacts to a topological insulator (TI) remain a persistent challenge on the route to engineer topological superconductivity. Recently, the higher-order TI WTe_2 was shown to turn superconducting when placed on palladium (Pd) bottom contacts, demonstrating a promising material system in pursuing this goal. Here, we report the diffusion of Pd into WTe_2 and the formation of superconducting $PdTe_x$ as the origin of observed superconductivity. We find an atomically sharp interface in the direction vertical to the van der Waals layers between the diffusion crystal and its host crystal, forming state-of-the-art superconducting contacts to a TI. The diffusion is discovered to be nonuniform along the width of the WTe_2 crystal, with a greater extent along the edges compared to the bulk. The potential of this contacting method is highlighted in transport measurements on Josephson junctions by employing external superconducting leads.

DOI: 10.1103/PhysRevMaterials.6.L081201

Introduction. Topological insulators (TIs) are insulating in the bulk while hosting gapless boundary states in which the spin of the electron is locked to its momentum [1]. When brought in contact with an *s*-wave superconductor, a novel pairing mechanism is predicted with Cooper pairs that resemble an effectively spinless superconductor [2,3]. Such topological superconductors could host Majorana bound states, the elementary building block of fault-tolerant quantum bits [4].

Fundamental to this approach is a highly transparent interface between the superconductor and topological insulator [5] through which the boundary states are proximitized. Even with state-of-the-art nanofabrication it remains challenging to create such pristine material interfaces as oxidation [6–9], contamination, and rough crystal interfaces introduce defects and therefore decrease contact transparency [10].

The van der Waals (vdW) material WTe_2 is predicted to be a higher-order TI [11–15], hosting topological edge states at its crystal hinges. It was recently shown that thin crystals of the material placed on top of palladium (Pd) bottom contacts turn superconducting [16], with a pronounced flow of supercurrent along the edges of a Josephson junction (JJ) formed out of this material system [17].

Here, we report diffusion of Pd into the WTe_2 forming superconducting $PdTe_x$ as the origin of superconductivity in the WTe_2/Pd system. The interface between $PdTe_x$ and WTe_2 in the direction vertical to the vdW layers is found to be atomically sharp, eliminating crystal-roughness between the superconductor and the higher-order TI completely. We further investigate the formation of $PdTe_x$ along the width of the WTe_2 host crystal and find it to be nonuniform, with a greater extent along the edges compared to the bulk. The potential of this novel contacting method to WTe_2 is highlighted in transport measurements on JJs that show improved quality when contacted externally by an intrinsic superconductor.

Pd diffusion in WTe_2. We begin with describing the general structure of WTe_2 Josephson junctions formed with Pd. Fabrication starts with patterning parallel lines of Pd on *p*-doped Si substrates with 285 nm of SiO_2 on top. Next, the vdW materials hexagonal boron nitride (hBN) and WTe_2 are exfoliated and afterwards stacked on top of the Pd bottom contacts, using a standard dry pickup technique [18]. Until full encapsulation with hBN, WTe_2 is handled inside an inert glovebox atmosphere to protect the material from oxidation [6–8]. After the stacking process, the polymer stamp is separated from the stacked device by heating the sample to 155 °C for ≈10 min. The remaining polymer residues are chemically dissolved afterwards. Depending on the desired transport experiment, contact to WTe_2 is made either through

*martin.endres@unibas.ch
†christian.schoenenberger@unibas.ch

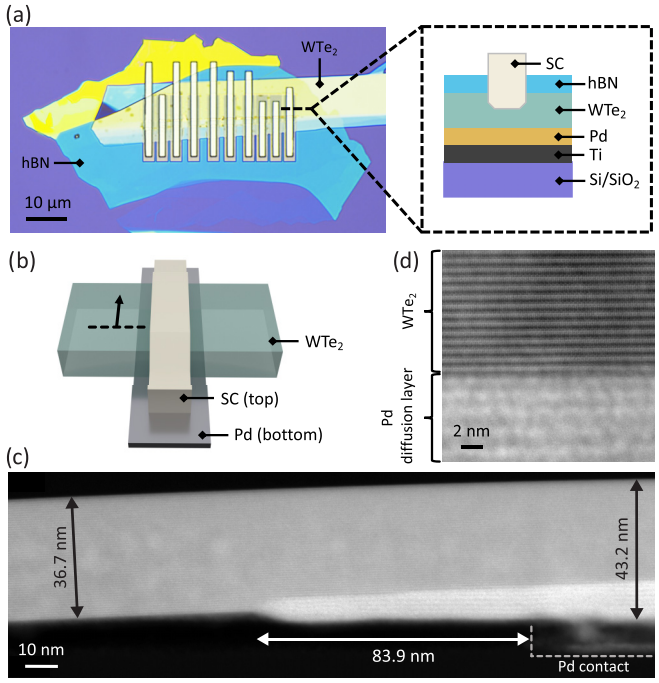

FIG. 1. Pd diffusion inside the WTe_2 crystal. (a) Left: Optical image of the elongated WTe_2 flake, covered with hBN on top of Pd contacts, with additional superconducting contacts (niobium) on top. Right: A schematic cross section of the device in a region of single Pd contact. (b) Illustration of the WTe_2 crystal on a single Pd bottom contact including a superconducting edge contact from the top. The direction of the cut lamella for the STEM image is indicated by the dashed line, and the viewing direction of the image is indicated by the arrow. (c) High-resolution STEM image taken at the edge of the Pd bottom contact (indicated by the gray dashed line at the bottom right). A bright diffusion layer at the interface between the Pd bottom contact and the WTe_2 crystal has formed. Black arrows indicate the thickness of the WTe_2 crystal, and the white arrow shows the lateral extent of diffusion in WTe_2 from the edge of the original Pd contact. (d) Zoom-in STEM image of the interface between the WTe_2 crystal and the diffusion layer.

the Pd bottom contacts or by etching through the covering top hBN and depositing superconducting contacts from the top. It should be noted that superconductivity is induced into WTe_2 by the Pd contacts alone [16,17] and that additional superconducting contacts are not required to form Josephson junctions. Figure 1(a) demonstrates an optical image of one of the devices. This device was prepared specially for electron microscopy, so additional top superconducting contacts do not have any practical purpose and are placed to replicate real transport devices. An extended description of the fabrication process can be found in the Supplemental Material [19–21].

In order to investigate the origin of superconductivity in WTe_2 in contact with Pd, we conduct high-resolution scanning transmission electron microscopy (STEM) imaging of the interface region. The illustration in Fig. 1(b) indicates the direction of the extracted lamella by a dashed line and the viewing direction by a perpendicular arrow. Figure 1(c) presents the STEM image taken with a high-annular angular dark-field detector (HAADF) at the edge of a Pd bottom contact, reaching into the weak link of the junction. Visible at first glance is a bright layer that has formed at the interface between the Pd bottom contact and the WTe_2 crystal on top. Moreover, the original Pd contact in the bottom right corner of Fig. 1(c) appears hollow and faded out, suggesting that the bright layer in WTe_2 is a result of Pd diffusion from the contact.

The presence of the diffusion layer in WTe_2 creates a pronounced swelling of the crystal, as highlighted by two thickness measurements of the WTe_2 flake in Fig. 1(c): inside the junction and on top of the Pd bottom contact. For pristine WTe_2 we extract an interlayer spacing of $c \sim 7.4$ Å that agrees with the literature value [22,23]. Inside the diffusion layer the perceived layer spacing has doubled to $c \sim 14.8$ Å. We connect the change in the layer spacing with the formation of a new crystal structure at the interface of WTe_2 and Pd, rather than merely intercalation of the original crystal by Pd. The formation of a new structure is further supported by Fig. 1(d), where we see, that the transition between the newly formed crystal and WTe_2 is very sharp and takes place on a single-layer scale. We also would like to note that the diffusion forming the new structure is quite anisotropic. Laterally, along the vdW layers, the diffusion layer extends ∼84 nm while vertically, perpendicular to the vdW layers, it only reaches ∼16 nm at its maximum. The lateral diffusion inside the JJ can diminish the length of the JJ, which could be especially prominent for the shorter junctions.

In the next section we analyze the atomic composition of the diffusion layer using energy dispersive x-ray (EDX) analysis. Figure 2(a) on the left shows a STEM image taken at the position of a superconducting niobium (Nb) top contact in this device. For better orientation, the location is illustrated in Fig. 2(b). From the bottom to the top, the faded Pd bottom contact, the Pd diffusion layer adjacent to the pristine WTe_2 crystal, and the Nb top contact are visible. Towards the right, EDX spectra of the elements in this slab are shown. Nb (turquoise) and the sticking layer for the Pd bottom contacts and titanium (Ti) are at their expected positions. Qualitatively, the concentration of tungsten (W) and tellurium (Te), represented in red and orange, respectively, are maximal in the unchanged WTe_2 crystal but reduced in the diffusion layer. Pd (in blue) has diffused through the entire WTe_2 crystal and is the dominating element inside the structurally changed layer. The concentration of Pd at the position of the original bottom contact is diminished, suggesting that depletion of the available material stopped the further growth of the diffusion layer.

A quantitative analysis of the crystal composition is shown in Fig. 2(b), following a trace indicated by the red arrow in the STEM image in Fig. 2(a). The ratio of W:Te is ∼1:2 and remains the same throughout most of the thickness. For Pd, two distinct concentration levels are visible, a high level of ∼60% that coincides with the structurally changed lattice and a second, low level of ∼20% inside the preserved WTe_2 crystal. The ratio of Pd:Te ∼ 3:1 suggests that the diffusion layer is not one of the known superconductors PdTe or $PdTe_2$ [24–27]. In the unchanged WTe_2 crystal above, Pd likely intercalates the vdW layers. So possibly, a threshold concentration of Pd is required to trigger the crystallographic change, such that the vertical extention of the diffusion layer is determined by the interplay of available Pd and thermal activation energy.

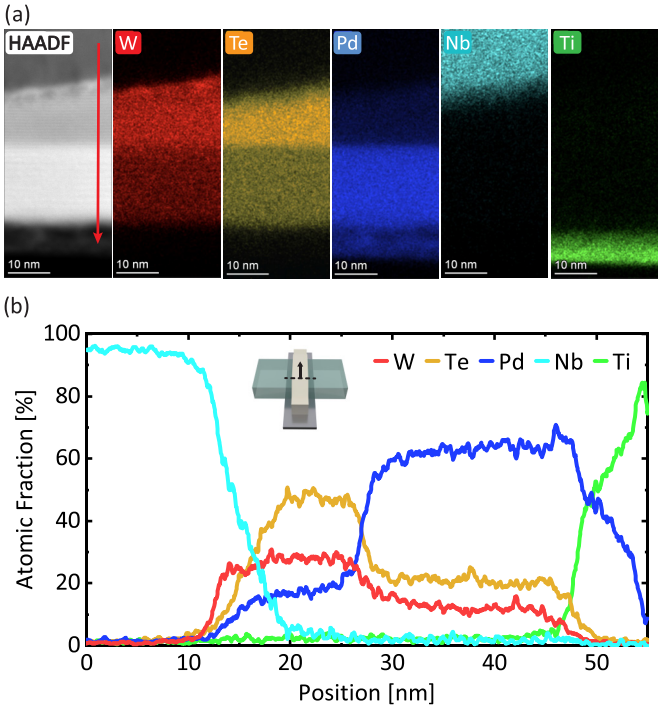

FIG. 2. EDX analysis of the Pd diffusion. (a) STEM image with the direction of the line cut in panel (b) indicated by a red arrow. Presented towards the right is the EDX analysis with elements existent in the device. Moving from the bottom to the top, the Pd bottom contact is followed by highly Pd interspersed WTe_2 layer that has structurally changed. Above, the crystal transitions sharply into the original crystal structure. (b) EDX line cut along the direction indicated in panel (a), with the position of the investigated lamella marked in the insert. Pd has diffused in the vertical direction through the entire WTe_2 crystal, with a sharp concentration increase in the structurally changed area that coincides with the STEM image.

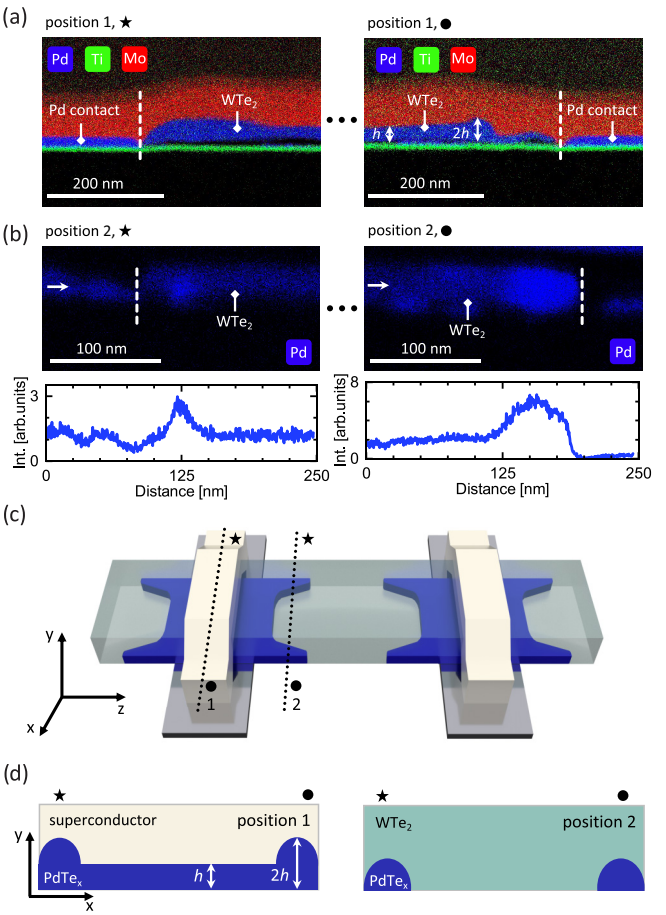

FIG. 3. Enhanced Pd diffusion along the edges of the WTe_2 crystal. (a) EDX analysis of a cross section taken on the Pd contact along position 1, as indicated in the schematics in panel (c). The given sample was equipped with a superconducting MoRe contact, evidenced by the Mo EDX signal in red. The left and right images correspond to the crystal edges marked by ⋆ and ● in the schematics, respectively. Visible is the swelling of WTe_2 to a thickness of $\sim 2h$ at the edge, compared to the bulk thickness of $\sim h$, indicated in the right image. (b) EDX signal and extracted intensity (Int.) profile taken towards the inside of the junction, indicated by position 2 in panel (c). The left and right images correspond to positions ⋆ and ● of the WTe_2 crystal, respectively. Visible in the EDX data is an increased intensity of the Pd signal at the edges of the crystal compared to the bulk. The increased Pd concentration is also visible by the enhanced EDX signal in the line cuts taken along the direction pointed out by the horizontal arrow. (c) Illustration of the inhomogeneous diffusion profile of $PdTe_x$ inside the WTe_2 host crystal. The self-formed $PdTe_x$ layer is drawn in blue inside the host crystal. (d) Cross-sectional cuts through the illustration along positions 1 and 2 in panel (c). The edges are marked by ⋆ and ● for orientation.

The remaining Pd concentration above the $PdTe_x$ layer quickly decays in the direction parallel to the vdW layers and extends ∼50 nm laterally beyond the structurally changed diffusion layer, as shown in Ref. [19].

Diffusion along the edges. Further, we investigate the uniformity of the $PdTe_x$ diffusion layer along the width of the Josephson junction. For this, we have analyzed several lamellas that are oriented perpendicular to the direction of the current in the JJ. The regions near the physical edges of WTe_2 are of particular interest, since additional Pd is available there due to the Pd bottom contacts extending beyond the crystal.

The first lamella was cut out through the middle of the bottom Pd contact in a sample with additional, this time molybdenum-rhenium (MoRe), top contacts, as illustrated by position 1 in Fig. 3(c). Figure 3(a) presents two EDX spectra obtained at the two edges marked by ⋆ and ● in Fig. 3(c). Outside of the WTe_2 flake we observe a layer of Pd with uniform thickness sandwiched between the MoRe top layer and the Ti bottom layer. Interestingly, inside WTe_2 near the edges, the thickness h of the $PdTe_x$ diffusion layer increases within a region of ∼100 nm away from the edge, as marked in the right spectrum of Fig. 3(a). Further from the edges, Pd is evenly distributed throughout the WTe_2 crystal. The difference of $PdTe_x$ thickness on the edges and in the middle of WTe_2 reaches a factor of ∼2.

The increase in thickness of $PdTe_x$ near the edges can be intuitively explained taking into account the fabrication procedure. During the last step of stacking, when the substrate is heated up to 155 °C to release the hBN/WTe_2 stack, the formation of the $PdTe_x$ takes place. In WTe_2 far away from the edges this process stops before reaching the full thickness of

the flake due to the depletion of available Pd. Near the edges, due to the availability of additional Pd, this process continues potentially even through the whole thickness of WTe_2. Afterwards, the top WTe_2 layers, not transformed to $PdTe_x$, are etched away during CHF_3/O_2 plasma etching of hBN prior to the deposition of the superconductor. This explanation is further corroborated by the uniform Pd concentration in Fig. 3(a) in contrast with the step in concentration in Fig. 2(b).

The increased Pd availability on the edges of the WTe_2 has the potential not only to increase the $PdTe_x$ thickness, but also to provide further diffusion inside the Josephson junction. To check this, we made a second lamella from another sample, which is cut inside the Josephson junction close to the end of Pd bottom contact, as shown as position 2 in Fig. 3(c). Visible in the EDX spectrum in Fig. 3(b) is an elevated intensity of Pd compared to the bulk at both ends of the crystal, highlighted by line cuts through the spectra along the horizontal arrows. This indicates that $PdTe_x$ is indeed penetrating further inside the junction along the edges of WTe_2 as visualized in Fig. 3(c).

We can roughly estimate the extent of the $PdTe_x$ diffusion along the edges, assuming that an increase by a factor of 2 in thickness h of $PdTe_x$ on the edges, as compared to the bulk [see Fig. 3(d)], yields the same increase in the diffusion inside the JJ along the edge. Taking from Fig. 1(c) that the $PdTe_x$ layer extends ∼85 nm inside the junction in the bulk, we would expect it to extend ∼170 nm along the edges. This diffusion could generate signatures of "artificial" edge supercurrents not due to a topological state. Nonetheless, evidence of topological hinge states in WTe_2 has been observed in combination with superconducting niobium contacts [15,28], where no edge diffusion is expected.

Josephson junction with fully superconducting contacts. During the formation of $PdTe_x$ in WTe_2 the majority of the Pd from the bottom contacts is depleted (see Figs. 1–3), thus creating a low-quality interface between bottom contacts and the newly formed Josephson junction. In this section we demonstrate a method to harness the full potential of the high-quality Josephson junction formed in WTe_2 with Pd diffusion by employing additional superconducting contacts from the top.

The fabrication process follows the description in Sec. II. After obtaining the stack, superconducting leads are patterned via standard *e*-beam lithography and sputtered onto the sample after etching through the top hBN with CHF_3/O_2 plasma. Prior to the deposition of MoRe superconducting leads, we perform a short Ar milling inside the sputtering chamber to remove the oxide layer from WTe_2. In order to avoid degradation of the JJs due to etching, the superconducting top contacts are separated by a distance of $l_{Pd} \sim 0.5$ μm from the edge of the Pd bottom contacts, as indicated in the schematics in Fig. 4(a). Figure 4(a) shows a finished device with top MoRe leads and its fabricated layer sequence to the right.

Measurement of the device is performed in a quasi-four-terminal setup, illustrated in Fig. 4(a). In this configuration, the measured differential resistance includes the contribution from the Josephson junction and the resistances of the interfaces between the MoRe and superconducting $PdTe_x$, but excludes the line resistances in the cryostat. Figures 4(b) and 4(c) show the $dV/dI(I)$ and $V(I)$ dependencies, measured on a 1-μm-long Josephson junction, with their behavior being representative for a number of samples we have studied. The curves reveal several abrupt transitions with current. Steps at $I \sim \pm 11$ μA have minimal hysteresis and correspond to the switching of superconducting $PdTe_x$ to the normal state or alternatively to a Josephson junction that has potentially formed at the interface of the vdW stack with MoRe [29].

The observed vanishing resistance at low bias currents by itself is not sufficient to ensure that the fabricated device performs indeed as a JJ. Potentially, the inhomogeneous diffusion of $PdTe_x$ could lead to a closed superconducting path through the weak link. In order to rule out this option, we study the dependence of dV/dI on the bias current I and the perpendicular magnetic field B, as shown in Fig. 4(d). Visible is a periodic "Fraunhofer"-like interference pattern that is a key signature of the Josephson effect. The oscillation periodicity $\delta B = 0.13$ mT is connected to a flux quantum Φ_0 threading the effective junction area $A_{\text{eff}} = w \times \ell_{\text{eff}}$, with $w = 4.3$ μm being the width of the junction and ℓ_{eff} being the effective length. The calculated $\ell_{\text{eff}} \sim 3.8$ μm exceeds the physical junction length of ∼1 μm. However, it can be explained by the contact geometry, assuming that half of the magnetic flux through the superconducting contacts is screened into the junction [30]. Additionally, a close look at the amplitude of consecutive lobes reveals a nonmonotonous behavior, reminiscent of an even-odd effect. A nonsinusoidal current phase relation of the junction [17] or an inhomogeneous current distribution [30], originating from the diffusion profile of $PdTe_x$, can create this feature.

Having established the Josephson effect through WTe_2, we take a closer look at the lower-current behavior observed in Figs. 4(b) and 4(c). First, in the superconducting branch of the JJ, the differential resistance is zero, implying that there is no measurable contribution of the MoRe/$PdTe_x$ interfaces. Second, in contrast to the previously studied devices with solely Pd leads [17], the switching behavior is highly hysteretic. The transition from the superconducting to the resistive branch, denoted by the switching current I_c, takes place at absolute current values higher than those of the transition in the opposite sweep direction, denoted by the retrapping current I_r, highlighted in Fig. 4(b).

Even though the hysteretic switching of the Josephson junction is most commonly explained by the junction being in the underdamped regime [31], we would argue that in our case overheating [32,33] plays the dominating role. Starting from the superconducting branch, no heat is dissipated in the Josephson junction before switching to the resistive branch. In contrast, lowering the bias current from the resistive branch includes dissipation of heat in the normal weak link, leading to a higher electron temperature. This explanation is corroborated by the temperature dependence of I_c and I_r shown in Fig. 4(e). Moving from high towards low temperatures, I_c and I_r both increase continuously down to $T \sim 220$ mK, when I_r begins to saturate while I_c remains increasing. Furthermore, this explanation is additionally supported by the devices with only Pd contacts. There, due to the normal Pd contacts remaining dissipative at all times, I_c saturates at low temperatures, as shown in Fig. 4(f).

Next, we characterize the quality of the $PdTe_x/WTe_2$ interface. Compared to conventional superconducting contacts

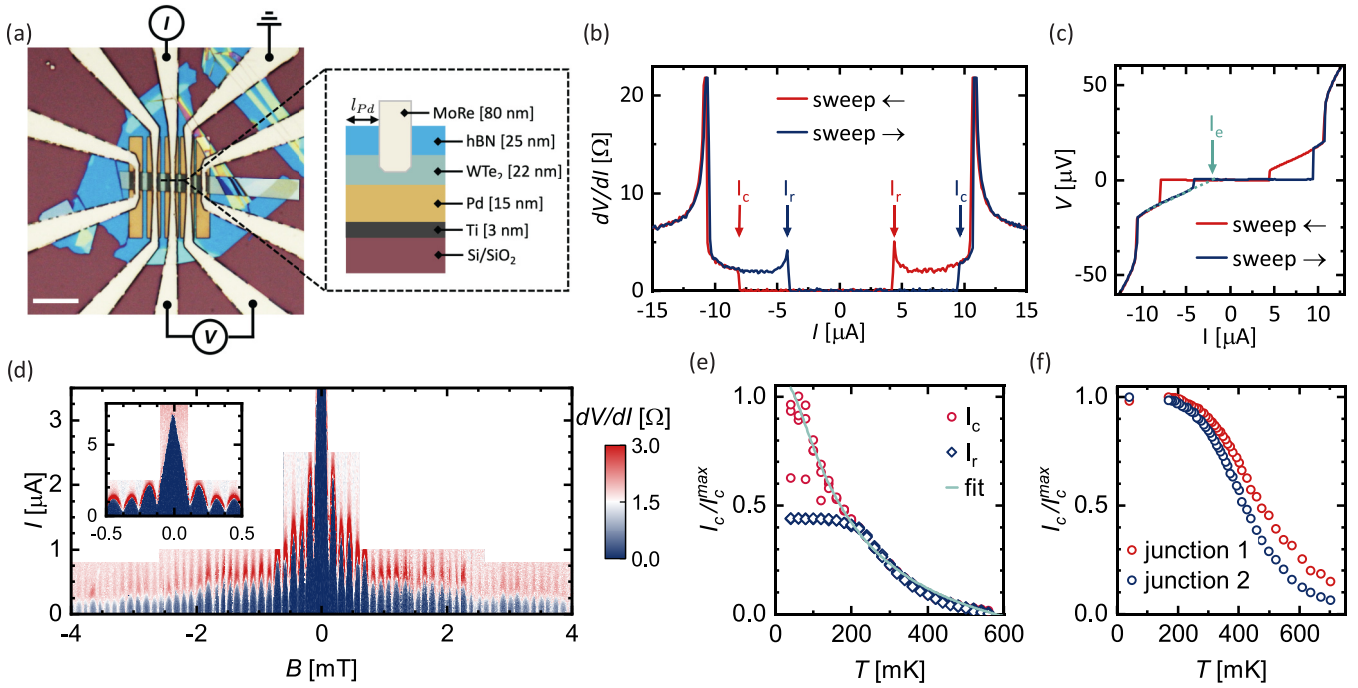

FIG. 4. Switching characteristics of Josephson junctions with superconducting or normal leads. (a) Optical image of the device with an illustration of the quasi-four-terminal measurement setup. The fabricated layer sequence is shown on the right. The scale bar is 10 μm. (b) dV/dI curves at the zero magnetic field of a JJ with superconducting contacts for two different sweep directions of the bias current. The hysteretic switching current depending on the sweep direction is visible from the shift of the critical current I_c and the retrapping current I_r. (c) $V(I)$ curves corresponding to the data in panel (b). The excess current I_e is evaluated from the intersection of the extended $V(I)$ curve to zero voltage. (d) dV/dI as a function of the bias current I and the perpendicular magnetic field B, following the "Fraunhofer" pattern expected for a Josephson junction. The insert shows the full range of the central lobe around $B = 0$. (e) Temperature dependence of the switching and retrapping currents I_c and I_r, respectively, of the same device as in panel (b). The data $I_c(T)$ are fitted in the scope of a diffusive long junction, plotted in light green. (f) Switching current I_c as a function of temperature T for two different JJs that are contacted only through Pd bottom contacts.

to WTe_2, the Josephson effect in junctions formed by Pd interdiffusion is found to be more robust in terms of junction length and magnetic field resilience [17]. Additionally, due to reduced heating effects, the here proposed devices support a critical current density twice as large compared to conventional contacts [28] at four times the junction length. The 1-μm-long junction presented in Fig. 4(b) maintains the Josephson effect with a critical current density j_c of up to $j_c > 10^8$ Am^{-2}, while comparable junctions with an even shorter length of up to 230 nm and conventional superconducting contacts are found to be limited by $j_c \sim 1 \times 10^7$ Am^{-2} – 5×10^7 Am^{-2} [28].

Further, from Fig. 4(e) we see that I_c is suppressed at 0.6 K, which is lower than the critical temperature $T_c = 1.2$ K [16] of the formed $PdTe_x$. We connect this reduction with the great length of the junction and fit for this reason $I_c(T)$ with an expression for a long diffusive junction [32,34]

$$I_c = \eta \frac{aE_{\mathrm{Th}}}{eR_N}\left[1 - b\exp\left(\frac{-aE_{\mathrm{Th}}}{3.2k_BT}\right)\right]. \quad (1)$$

Here, a and b are constants equal to 10.82 and 1.30, respectively, k_B is the Boltzmann constant, and E_{Th} is the Thouless energy. The empirical prefactor $\eta \in [0, 1]$ can be interpreted as a measure for the interface quality, scaling the maximum I_c. The data in Fig. 4(e) are well described by the model, which yields $\eta = 0.5$ and $E_{\mathrm{Th}} = 3.87$ μeV. A similar fit procedure for the data in Fig. 4(f), obtained from a junction with only Pd contacts, is not reliable as I_c ($T < 400$ mK) is limited by heating effects and deviates strongly from the theoretical prediction.

The evaluation of the interface transparency is corroborated by the excess current I_e, extracted from the $V(I)$ curve in Fig. 4(c). We extrapolate I_e after the transition from the superconducting to the resistive branch and obtain [35] $I_eR_N/\Delta \sim 0.03$, using $\Delta = 1.76k_BT_c = 182$ μeV [16]. In the framework of the Octavio-Tinkham-Blonder-Klapwijk theory [36,37], this relates to a junction transparency of $T = 1/(1 + Z^2) \sim 0.5$, with $Z \sim 1.1$.

At this point we would like to comment on the role of R_N in the two analytical models of the preceding analysis yielding a transparency of ~0.5. The bulk conductivity of WTe_2 increases with flake thickness [38]. These additional bulk modes in the normal state shunt R_N, but do not participate in superconducting transport of the long junction due to their fast decay $I_{c,\mathrm{bulk}} \propto \ell_{\mathrm{mfp}}^2/L_w^3$, compared to ballistic edge modes $I_{c,\mathrm{edge}} \propto 1/L_w$ [39], with ℓ_{mfp} being the electronic mean free path. This phenomenon has also been reported in JJs formed of the topological material Bi_2Se_3 [40]. The extracted transparency is therefore systematically underestimated and serves only as a lower bound to the real value.

Conclusion. We have demonstrated a robust method to form atomically sharp superconducting contacts to WTe_2 mediated by Pd diffusion during stacking. Josephson junctions formed by these contacts are highly transparent. Given recent reports of similar processes in BiSbTe [35,41] this method could be a promising approach for other topological candidates based on Te compounds. We have further demonstrated that the diffusion inside the host crystal could be nonuniform, generating false signatures of superconducting edge currents. Therefore, caution has to be exercised in the evaluation of a diffusion-driven Josephson junction when assigning it to a topological superconductor. Furthermore, we have proposed a method to avoid overheating in transport through Pd-diffusion-mediated Josephson junctions by employing additionally superconducting leads.

Note added. Recently we became aware of a publication [42] that also demonstrates the interdiffusion of Pd into WTe_2, with the formation of PdTe leading to superconductivity.

All data in this publication are available in numerical form in the Zenodo repository [43].

Acknowledgments. We thank Paritosh Karnatak for fruitful discussions. This project has received funding from the European Research Council (ERC) under the European Unions Horizon 2020 research and innovation programme, Grant No. 787414 TopSupra; from the Swiss National Science Foundation through the National Centre of Competence in Research Quantum Science and Technology (QSIT); and from the Swiss Nanoscience Institute (SNI). A.K. was supported by the Georg H. Endress Foundation. D.M. and J.Y. acknowledge support from the U.S. Department of Energy (U.S. DOE), Office of Science, Basic Energy Sciences (BES), Materials Sciences and Engineering Division. H.S.A. was supported by the Gordon and Betty Moore Foundation's EPiQS Initiative through Grant No. GBMF9069 and the Shull Wollan Center Graduate Research Fellowship. D.M. acknowledges support from the Gordon and Betty Moore Foundation's EPiQS Initiative, Grant No. GBMF9069. K.W. and T.T. acknowledge support from the Elemental Strategy Initiative conducted by MEXT, Japan, and the CREST (Grant No. JPMJCR15F3), JST.

M.E. has fabricated the devices. M.E. and A.K. measured the devices in transport. M.S. and M.W. performed the STEM and EDX imaging. H.S.A., J.Y., and D.M. provided the WTe_2 crystals. K.W. and T.T. provided hBN crystals. M.E., A.K., and C.S. analyzed the data and wrote the manuscript.

The authors declare no competing interests.

[1] L. Fu and C. L. Kane, Topological insulators with inversion symmetry, Phys. Rev. B **76**, 045302 (2007).

[2] L. Fu and C. L. Kane, Superconducting Proximity Effect and Majorana Fermions at the Surface of a Topological Insulator, Phys. Rev. Lett. **100**, 096407 (2008).

[3] C. W. Beenakker, Search for majorana fermions in superconductors, Annu. Rev. Condens. Matter Phys. **4**, 113 (2013).

[4] T. Hyart, B. Van Heck, I. C. Fulga, M. Burrello, A. R. Akhmerov, and C. W. J. Beenakker, Flux-controlled quantum computation with Majorana fermions, Phys. Rev. B **88**, 035121 (2013).

[5] P. Schüffelgen, D. Rosenbach, C. Li, T. W. Schmitt, M. Schleenvoigt, A. R. Jalil, S. Schmitt, J. Kölzer, M. Wang, B. Bennemann, U. Parlak, L. Kibkalo, S. Trellenkamp, T. Grap, D. Meertens, M. Luysberg, G. Mussler, E. Berenschot, N. Tas, A. A. Golubov *et al.*, Selective area growth and stencil lithography for in situ fabricated quantum devices, Nat. Nanotechnol. **14**, 825 (2019).

[6] F. Ye, J. Lee, J. Hu, Z. Mao, J. Wei, and P. X.-L. Feng, Environmental instability and degradation of single- and few-layer WTe_2 nanosheets in ambient conditions, Small **12**, 5802 (2016).

[7] H. Liu, N. Han, and J. Zhao, Atomistic insight into the oxidation of monolayer transition metal dichalcogenides: From structures to electronic properties, RSC Adv. **5**, 17572 (2015).

[8] F. Hou, D. Zhang, P. Sharma, S. Singh, T. Wu, and J. Seidel, Oxidation kinetics of WTe_2 surfaces in different environments, ACS Appl. Electron. Mater. **2**, 2196 (2020).

[9] C. R. Thomas, M. K. Vallon, M. G. Frith, H. Sezen, S. K. Kushwaha, R. J. Cava, J. Schwartz, and S. L. Bernasek, Surface oxidation of $Bi_2(Te,Se)_3$ topological insulators depends on cleavage accuracy, Chem. Mater. **28**, 35 (2016).

[10] P. F. Bagwell, Suppression of the Josephson current through a narrow, mesoscopic, semiconductor channel by a single impurity, Phys. Rev. B **46**, 12573 (1992).

[11] F. Schindler, A. M. Cook, M. G. Vergniory, Z. Wang, S. S. P. Parkin, B. A. Bernevig, and T. Neupert, Higher-order topological insulators, Sci. Adv. **4**, eaat0346 (2018).

[12] W. A. Benalcazar, B. A. Bernevig, and T. L. Hughes, Quantized electric multipole insulators, Science **357**, 61 (2017).

[13] Z. Wang, B. J. Wieder, J. Li, B. Yan, and B. A. Bernevig, Higher-Order Topology, Monopole Nodal Lines, and the Origin of Large Fermi Arcs in Transition Metal Dichalcogenides XTe_2 (X = Mo, W), Phys. Rev. Lett. **123**, 186401 (2019).

[14] L. Peng, Y. Yuan, G. Li, X. Yang, J.-J. Xian, C.-J. Yi, Y.-G. Shi, and Y.-S. Fu, Observation of topological states residing at step edges of WTe_2, Nat. Commun. **8**, 659 (2017).

[15] C. Huang, A. Narayan, E. Zhang, X. Xie, L. Ai, S. Liu, C. Yi, Y. Shi, S. Sanvito, and F. Xiu, Edge superconductivity in multilayer WTe_2 Josephson junction, Natl. Sci. Rev. **7**, 1468 (2020).

[16] A. Kononov, M. Endres, G. Abulizi, K. Qu, J. Yan, D. G. Mandrus, K. Watanabe, T. Taniguchi, and C. Schönenberger, Superconductivity in type-II Weyl-semimetal WTe_2 induced by a normal metal contact, J. Appl. Phys. **129**, 113903 (2021).

[17] A. Kononov, G. Abulizi, K. Qu, J. Yan, J. Yan, D. Mandrus, D. Mandrus, K. Watanabe, T. Taniguchi, and C. Schönenberger, One-dimensional edge transport in few-layer WTe_2, Nano Lett. **20**, 4228 (2020).

[18] P. J. Zomer, M. H. Guimarães, J. C. Brant, N. Tombros, and B. J. Van Wees, Fast pick up technique for high quality heterostructures of bilayer graphene and hexagonal boron nitride, Appl. Phys. Lett. **105**, 013101 (2014).

[19] See Supplemental Material at http://link.aps.org/supplemental/10.1103/PhysRevMaterials.6.L081201 for detailed description of the fabrication process and additional EDX analysis.

[20] P. Blake, E. W. Hill, A. H. Castro Neto, K. S. Novoselov, D. Jiang, R. Yang, T. J. Booth, and A. K. Geim, Making graphene visible, Appl. Phys. Lett. **91**, 063124 (2007).

[21] Y. Zhao, H. Liu, J. Yan, W. An, J. Liu, X. Zhang, H. Wang, Y. Liu, H. Jiang, Q. Li, Y. Wang, X. Z. Li, D. Mandrus, X. C. Xie, M. Pan, and J. Wang, Anisotropic magnetotransport and exotic longitudinal linear magnetoresistance in WTe_2 crystals, Phys. Rev. B **92**, 041104(R) (2015).

[22] B. E. Brown, The crystal structures of WTe_2 and high-temperature $MoTe_2$, Acta Crystallogr. **20**, 268 (1966).

[23] T.-R. Chang, S-Y. Xu, G. Chang, C.-C. Lee, S.-M. Huang, B. K. Wang, G. Bian, H. Zheng, D. S. Sanchez, I. Belopolski, N. Alidoust, M. Neupane, A. Bansil, H.-T. Jeng, H. Lin, and M. Zahid Hasan, Prediction of an arc-tunable Weyl Fermion metallic state in $Mo_xW_{1-x}Te_2$, Nat. Commun. **7**, 10639 (2016).

[24] A. Karki, D. Browne, S. Stadler, J. Li, and R. Jin, PdTe: A strongly coupled superconductor, J. Phys.: Condens. Matter **24**, 055701 (2012).

[25] B. Tiwari, R. Goyal, R. Jha, A. Dixit, and V. Awana, PdTe: a 4.5 K type-II BCS superconductor, Supercond. Sci. Technol. **28**, 055008 (2015).

[26] S. Das, Amit, A. Sirohi, L. Yadav, S. Gayen, Y. Singh, and G. Sheet, Conventional superconductivity in the type-II Dirac semimetal $PdTe_2$, Phys. Rev. B **97**, 014523 (2018).

[27] J. A. Voerman, J. C. de Boer, T. Hashimoto, Y. Huang, C. Li, and A. Brinkman, Dominant *s*-wave superconducting gap in $PdTe_2$ observed by tunneling spectroscopy on side junctions, Phys. Rev. B **99**, 014510 (2019).

[28] Y. B. Choi, Y. Xie, C. Z. Chen, J. Park, S. B. Song, J. Yoon, B. J. Kim, T. Taniguchi, K. Watanabe, J. Kim, K. C. Fong, M. N. Ali, K. T. Law, and G. H. Lee, Evidence of higher-order topology in multilayer WTe_2 from Josephson coupling through anisotropic hinge states, Nat. Mater. **19**, 974 (2020).

[29] M. R. Sinko, S. C. de la Barrera, O. Lanes, K. Watanabe, T. Taniguchi, S. Tan, D. Pekker, M. Hatridge, and B. M. Hunt, Superconducting contact and quantum interference between two-dimensional van der Waals and three-dimensional conventional superconductors, Phys. Rev. Materials **5**, 014001 (2021).

[30] S. Ghatak, O. Breunig, F. Yang, Z. Wang, A. A. Taskin, and Y. Ando, Anomalous Fraunhofer patterns in gated Josephson junctions based on the bulk-insulating topological insulator $BiSbTeSe_2$, Nano Lett. **18**, 5124 (2018).

[31] M. Tinkham, *Introduction to Superconductivity*, 2nd ed. (Dover, New York, 2004).

[32] A. De Cecco, K. Le Calvez, B. Sacépé, C. B. Winkelmann, and H. Courtois, Interplay between electron overheating and ac Josephson effect, Phys. Rev. B **93**, 180505(R) (2016).

[33] H. Courtois, M. Meschke, J. T. Peltonen, and J. P. Pekola, Origin of Hysteresis in a Proximity Josephson Junction, Phys. Rev. Lett. **101**, 067002 (2008).

[34] P. Dubos, H. Courtois, B. Pannetier, F. K. Wilhelm, A. D. Zaikin, and G. Schön, Josephson critical current in a long mesoscopic S-N-S junction, Phys. Rev. B **63**, 064502 (2001).

[35] M. Bai, F. Yang, M. Luysberg, J. Feng, A. Bliesener, G. Lippertz, A. A. Taskin, J. Mayer, and Y. Ando, Novel self-epitaxy for inducing superconductivity in the topological insulator $(Bi_{1-x}Sb_x)_2Te_3$, Phys. Rev. Materials **4**, 094801 (2020).

[36] M. Octavio, M. Tinkham, G. E. Blonder, and T. M. Klapwijk, Subharmonic energy-gap structure in superconducting constrictions, Phys. Rev. B **27**, 6739 (1983).

[37] K. Flensberg, J. B. Hansen, and M. Octavio, Subharmonic energy-gap structure in superconducting weak links, Phys. Rev. B **38**, 8707 (1988).

[38] F.-X. Xiang, A. Srinivasan, Z. Z. Du, O. Klochan, S.-X. Dou, A. R. Hamilton, and X.-L. Wang, Thickness-dependent electronic structure in WTe_2 thin films, Phys. Rev. B **98**, 035115 (2018).

[39] A. Murani, A. Kasumov, S. Sengupta, Y. A. Kasumov, V. Volkov, I. Khodos, F. Brisset, R. Delagrange, A. Chepelianskii, R. Deblock, H. Bouchiat, and S. Guéron, Ballistic edge states in bismuth nanowires revealed by squid interferometry, Nat. Commun. **8**, 15941 (2017).

[40] L. Galletti, S. Charpentier, M. Iavarone, P. Lucignano, D. Massarotti, R. Arpaia, Y. Suzuki, K. Kadowaki, T. Bauch, A. Tagliacozzo *et al.*, Influence of topological edge states on the properties of $Al/Bi_2Se_3/Al$ hybrid Josephson devices, Phys. Rev. B **89**, 134512 (2014).

[41] M. Bai, X.-K. Wei, J. Feng, M. Luysberg, A. Bliesener, G. Lippertz, A. Uday, A. A. Taskin, J. Mayer, and Y. Ando, Proximity-induced superconductivity in $(Bi_{1-x}Sb_x)_2Te_3$ topological-insulator nanowires, Commun. Mater. **3**, 20 (2022).

[42] M. Ohtomo, R. S. Deacon, M. Hosoda, N. Fushimi, H. Hosoi, M. D. Randle, M. Ohfuchi, K. Kawaguchi, K. Ishibashi, and S. Sato, Josephson junctions of Weyl semimetal WTe_2 inducted by spontaneous nucleation of PdTe superconductor, Appl. Phys. Express **15**, 075003 (2022).

[43] Zenodo repository, https://doi.org/10.5281/zenodo.6556998.